



# Geochemical characterization of the gneisses and schists in Ekumtak area: further evidence for a metasedimentary protolith and moderate weathering intensity for the Precambrian Basement complex of Nigeria

Chinedu Uduma IBE<sup>1</sup>

**Resumen:** CARACTERIZACIÓN GEOQUÍMICA DE GNEIS Y ESquistos EN EL ÁREA DE EKUMTAK: MÁS EVIDENCIA DE UN PROTOLITO METASEDIMENTARIO Y UNA INTENSIDAD DE METEORIZACIÓN MODERADA PARA EL COMPLEJO DEL SÓTANO PRECÁMBRICO DE NIGERIA. El área de estudio se caracteriza por gneis con bandas migmatíticas y esquistos de mica granate. Estas rocas están asociadas con intrusiones graníticas y anfibolíticas. Estos gneis y esquistos migmatíticos se caracterizan por conjuntos de minerales paragenéticos que reflejan una historia evolutiva que involucró procesos de sedimentación y metamorfismo de facies de anfibolitas superiores. Los datos geoquímicos muestran que las rocas son ricas en sílice con concentraciones moderadas a elevadas de  $\text{Al}_2\text{O}_3$ , lo que es consistente con las rocas pelíticas. Los gneises muestran anomalías positivas en Rb, K, Th, La, Sm y fuertes anomalías negativas en Ta, Nb, Sr, Ti, Tm, Yb, Zr e Y, con un enriquecimiento general de los elementos litófilos de iones grandes (LILE: K, Ba y Rb) y el agotamiento de los elementos de alta intensidad de campo (HFSE: Zr, Ti e Y). Específicamente, las Eu-anomalías, expresadas como  $(\text{Eu}/\text{Eu}^*)$  varían de 0.03 a 1.4 en los gneises y de 0.09 a 1.1 en los esquistos. Las relaciones  $\text{LaN}/\text{YbN}$  son de 7 a 93 para los gneises y de 1,9 a 46,4 para el esquisto. Estos valores sugieren que los protolitos de estas rocas metasedimentarias son predominantemente lutitas, grauvacas y areniscas arkósicas con componentes volcánicos surbodinados básicos a intermedios. Su índice químico de valores de alteración varía de 57.7 a 71.7 en los gneises y 66.6 a 74.9 en los esquistos con una media de 68% y una desviación estándar de  $\pm 3.4$ , lo que sugiere un proceso de reciclaje y una meteorización química relativamente moderada de los protolitos. El origen metasedimentario de las rocas es consistente con los resultados de otras partes del complejo del Sótano Precámbrico de Nigeria.

**Abstract:** The study area is characterized by migmatitic banded gneisses and garnet mica schists. These rocks are associated with amphibolite and granitic intrusions. These migmatitic gneisses and schists are characterized by paragenetic mineral assemblages that reflect an evolutionary history that involved processes of sedimentation and upper amphibolite facies metamorphism. Geochemical data show that the rocks are silica rich with moderate to elevated concentrations of  $\text{Al}_2\text{O}_3$ , which is consistent with pelitic rocks. The gneisses show positive anomalies in Rb, K, Th, La, Sm and strong negative anomalies in Ta, Nb, Sr, Ti, Tm, Yb, Zr and Y, with an overall enrichment of the large ion lithophile elements (LILE: K, Ba and Rb) and depletion of the high field strength elements (HFSE: Zr, Ti and Y). Specifically, the Eu-anomalies, expressed as  $(\text{Eu}/\text{Eu}^*)$  range from 0.03 to 1.4 in the gneisses and from 0.09 to 1.1 in the schists.  $\text{LaN}/\text{YbN}$  ratios are from 7 to 93 for the gneisses and 1.9 to 46.4 for the schist. These values suggest that the protoliths of these metasedimentary rocks are predominantly shales, greywackes and arkosic sandstones with subordinate basic to intermediate volcanic components. Their chemical index of alteration values ranges from 57.7-71.7 in the gneisses and 66.6-74.9 in the schists with mean of 68% and standard deviation of  $\pm 3.4$  suggesting a recycle process and relatively moderate chemical weathering of the protoliths. The metasedimentary origin for the rocks is consistent with results from other parts of the Nigerian Precambrian Basement complex.

<sup>1)</sup> Department of Geology, University of Nigeria, Nsukka, 410001, Nigeria. Corresponding author: chinedu.ibe@unn.edu.ng. +234 813 8655 078

**Palabras clave:** Gneis, Metamorfismo, Protolito, Precámbrico, Metasedimentario, Esquistos.

**Key words:** Gneisses, Metamorphism, Protolith, Precambrian, Metasedimentary, Schists.

## Introduction

The oldest basement rocks (ca. 3500 Ma) in West Africa are found at the southeastern border of the West African craton (Kroner *et al.*, 2001) (Figure 1). The West African terrane was affected by the Eburnean orogeny (ca.  $2000 \pm 150$  Ma) and consolidated as a craton during a period of tectonic quiescence between 1700 to 1000 Ma (Liègeois *et al.*, 2013).

Extensional events which were associated with continental break up affected the West African craton in the early Neoproterozoic (Liègeois *et al.*, 2013). These favored passive margin sedimentation with localized calc-alkaline volcanic occurrences and the development

of younger basement rocks, represented by pelitic to psammite terranes (Kinnaird, 1984).

During the Gondwana assembly, the West African craton (WAC) was subjected to convergence along its boundaries (Kinnaird, 1984). The eastern passive margin collided with the active margin of the Trans Saharan orogenic belt (TSOB) of which the Nigerian Precambrian Basement Complex is a part and lies between the WAC and the Congo-Gabon craton (Figure 1). The collision at this plate margin is believed to have led to the reactivation and remobilization of the internal region of the Pan-African belt and the Nigerian Precambrian Basement Complex (Ibe and Obiora, 2019).

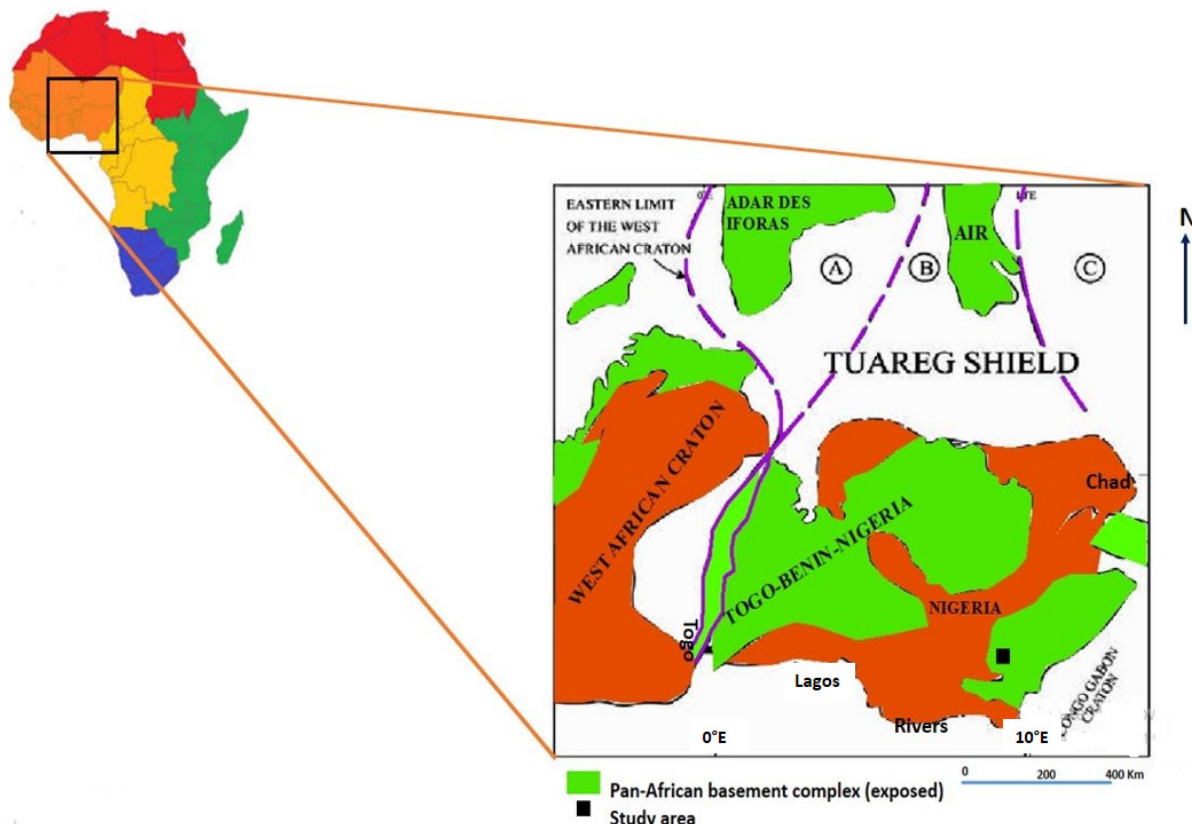


**Figure 1.** Location of the Precambrian Basement Complex in Nigeria between the West African craton, the Congo-Gabon craton and the southern part of the Tuareg shield./**Figura 1.** Ubicación del complejo del sótano Precámbrico en Nigeria entre el cratón de África occidental, el cratón Congo-Gabón y la parte sur del escudo Tuareg.

## Geological setting

The study area is located within the extension of the Bamenda highlands of Cameroun into southeastern Nigeria, otherwise referred to as the Bamenda massif or the southeastern Nigerian Precambrian Basement Complex (Obiora, 2006). The migmatitic rocks in the area were grouped together as “Granitoids” on the Geological Map of Nigeria produced by the Nigerian Geological Survey Agency (NGSA, 2011). The migmatitic character of the rocks reflects long, protracted and possibly polycyclic evolutionary history (Annor, 1998), which corroborates the four thermotectonic events that have affected the Nigerian Basement at various localities (Burke and Dewey, 1972). The present study was carried out because of the need for the mapping and delineation of the various rock types of the different units of the Precambrian Basement Complex in the area. It was also carried out because of the need for detailed petrographic and geochemical (major-, trace-, and rare-earth elements) studies on the migmatitic rocks and granitoids for proper assessment of their protoliths as well as their weathering history.

## Field relationship and petrographic characteristics of the rocks

The study area is characterized by migmatitic banded gneisses and garnet biotite schists. The gneisses constitute the Basement in strict sense and are either overlain or intruded by the other units. They generally have NNW-SSE trending gneissose foliation with few N-S trends and dip values which vary from as low as 10° to 35° in both NE and SW directions (Figure 2). The modal compositions of the rocks are presented in Table 1.

### Garnet-Biotite Schist (GBS)

This unit occurs in the eastern part of

the study area (Figure 2) and extends outside the map area to the eastern corner of the Kyikabe hills. It constitutes about 30% of the exposed rocks in the study area. The rock is medium grained, melanocratic and characterized by schistose foliation defined by the preferential alignment of the black-colored mineral (biotite). It also contains quartz and garnet. They are conspicuously melanocratic due to the preponderance of biotite in the rock. The exposure at Njuakaku hill is characterized by intense micro-folding of quartz-feldspar injections and ptygmatic folds (Figure 3a). Schistosity in most of the outcrops trends NW-SE to NE-SW.

### Migmatitic banded gneiss (MBGn)

This unit occurs in the western part of the study area. It is generally mesocratic, coarse grained and shows a well-defined gneissose foliation consisting of alternations of light-colored layers containing feldspars and quartz with dark colored layers containing biotite. The gneissose foliation trends essentially NNW-SSE and N-S with dips of 15 to 30° to the east and west. It possesses some qualities of migmatites such as the occurrence of mixtures of different rock types with quartz-feldspar veins. Generally, the migmatitic banded gneisses comprise both metamorphic host rock (paleosome) and leucocratic acid injections (leucosome). The leucosome commonly form layers or elongate thin lenses that are often concordant to the foliation of the paleosome giving the rock a banded appearance (Figure 3b). This unit also extends from the central to the southwestern parts of the area of study, stretching from Oku towards the south of Okundi, where it is characterized by porphyroblasts of garnet, feldspars and quartz which occasionally distort the gneissose foliation (Figure 3c). The exposure in Ekumtak hill is intensely exfoliated (Figure 3d). At Odajie-Mbube, which is located at about 9 km, northeast of Obawop, this unit is characterized by porphyroblasts of garnet, biotite and feldspars in a coarse-grained

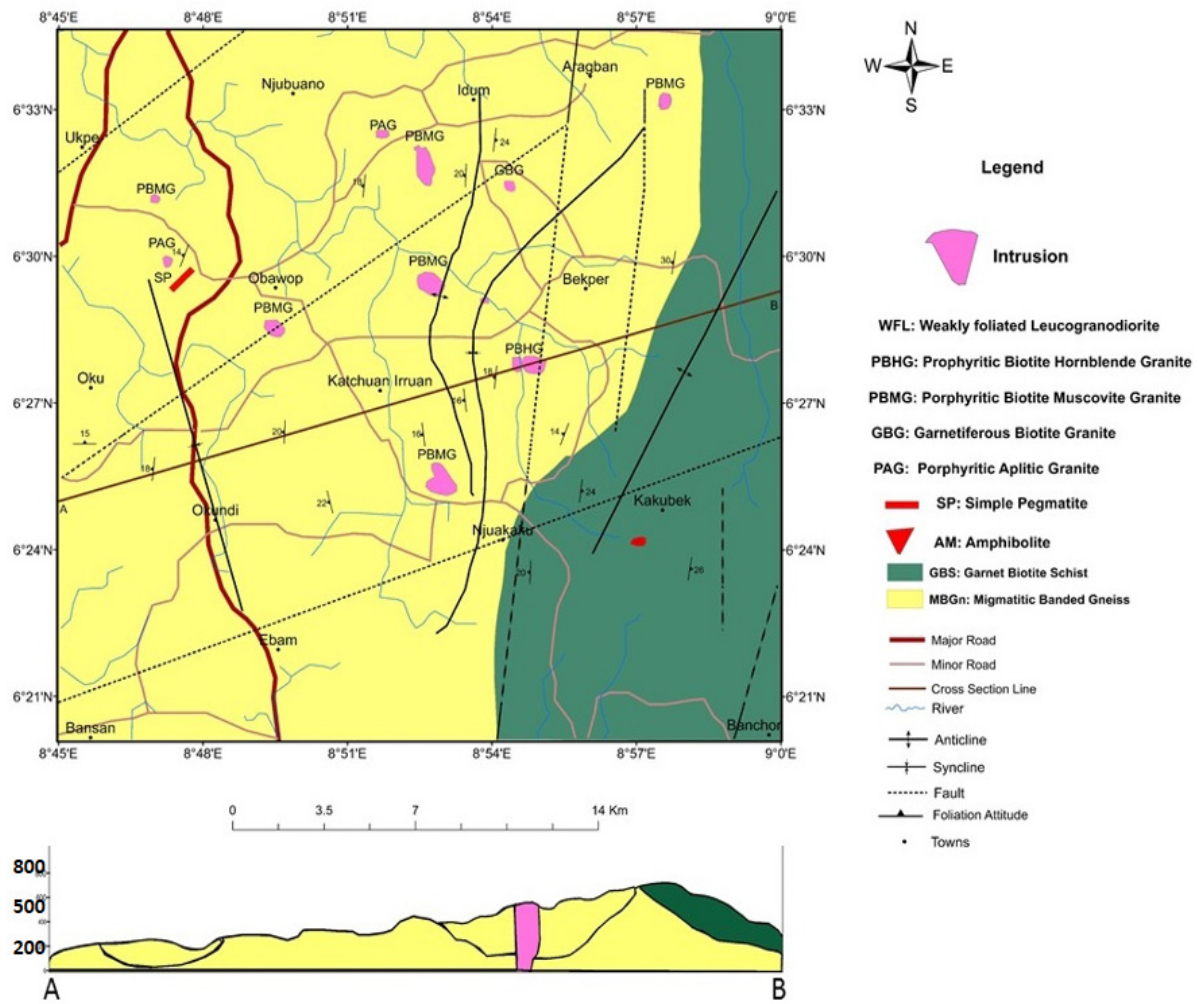


**Figure 2.** Geologic map of the study area./**Figura 2.** Mapa geológico del área de estudio.

groundmass of same minerals with sillimanite which was identified, particularly as stringers concentrated in the biotite-rich parts of the rock.

### Microscopic study

The minerals identified in the garnet biotite schists include quartz, andesine, garnet and muscovite. Some accessories include zircon and chlorite. In thin section, the schistose foliation is defined by the platy mineral, biotite. Other minerals that make up the rock include almandine garnet, quartz, microcline and plagioclase of An39 which is Andesine. For the banded gneisses, the melanocratic layers consist mainly of biotite, which is arranged in a parallel to sub-parallel manner (Figure 4a). The light-coloured layers, on the other hand contain feldspar, and quartz, with tiny specks of muscovite. Plagioclase occurs

in crystals of two different compositions from anorthite composition determination, viz: An<sub>8</sub> and An<sub>55</sub>, which are albite and labradorite, respectively (Figure 4b). The outcrops around Katchuan contains hornblende and sphene in addition. Sphene, as shown in thin section, has a high relief and occurs in euhedral crystals that have an acute rhombic cross section (Figure 4c). Hornblende measures about 3 mm and occurs in subidioblastic grains with inclusions of quartz and biotite (Figure 4d). Sillimanite is brown and occurs as fibrolite and small prismatic needles closely associated with biotite in sillimanite-biotite bands (Figure 4e). The growth of the porphyroblasts of garnet which measure about 8 mm in diameter and contains inclusions of quartz, biotite and opaque minerals, is accompanied by volume increase and the pushing away of the crystals of

**Table 1. Modal compositions of Precambrian Basement Gneisses (Gn 1-7) and Schists (Sh 1-6) of Bamenda massif, southeast of Ogoja, Southeastern Nigeria.**

Mineral	Gn1	Gn2	Gn3	Gn4	Gn5	Gn6	Gn7	Sh1	Sh2	Sh3	Sh4	Sh5	Sh6
Quartz	20	20	25	15	15	25	30	25	10	20	25	20	15
Plagioclase	10	30	10	30	25	15	15	30	20	20	20	25	10
Microcline	5	<1	<1	5	5	<1	5	10	5	<1	<1	5	5
Biotite	30	25	30	25	15	15	10	15	30	20	30	15	25
Garnet	<1	<1	<1	<1	15	30	<1	<1	10	15	20	20	25
Muscovite	10	5	<1	5	5	5	<1	<1	10	10	15	10	15
Hornblende	<1	5	<1	20	10	<1	25	<1	<1	<1	<1	<1	<1
Cordierite	10	5	<1	<1	<1	<1	<1	5	<1	<1	<1	<1	<1
Sillimanite	<1	<1	<1	<1	10	<1	<1	<1	<1	<1	<1	<1	<1
Sphene	<1	<1	20	<1	<1	<1	<1	<1	<1	<1	<1	<1	<1
Zircon	5	5	<1	<1	<1	<1	<1	5	5	5	<1	<1	5
Chlorite	5	<1	<1	<1	<1	<1	<1	5	5	5	5	5	<1
Sericite	5	5	10	10	<1	5	10	10	<1	5	5	<1	<1
Opaque	<1	<1	5	<1	<1	<1	<1	<1	5	<1	<1	<1	<1
Total	100	100	100	100	100	100	100	100	100	100	100	100	100

**Table 1.** Modal compositions of Precambrian Basement Gneisses and Schists of Bamenda massif, southeast of Ogoja, Southeastern Nigeria./*Tabla 1. Composiciones modales de gneises y esquistos del sótano Precámbrico del macizo de Bamenda, al sureste de Ogoja, sureste de Nigeria.*

quartz and biotite while most of the biotite crystals around the porphyroblasts seem to have been eaten up by the formation of the garnet (Figure 4f). Some plagioclase crystals also show combined albite-carlsbad twinning while some have been sericitized such that

their characteristic albite twinning have been almost obliterated (Figure 4g). Myrmekitic intergrowths are also observed in the rock (Figure 4h). The texture of garnet is poikiloblastic as it is riddled with inclusions of quartz and hematite (Figure 4i).

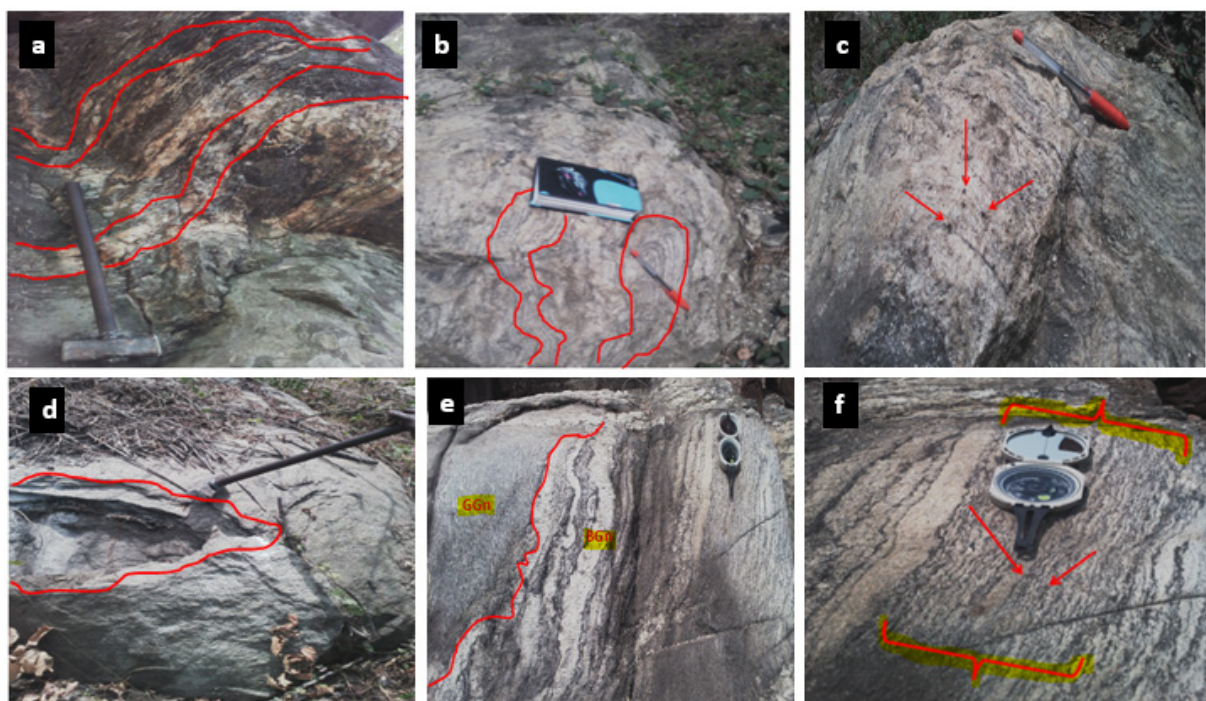


**Figure 3.** Field photographs./*Figura 3. Fotografías de campo.*

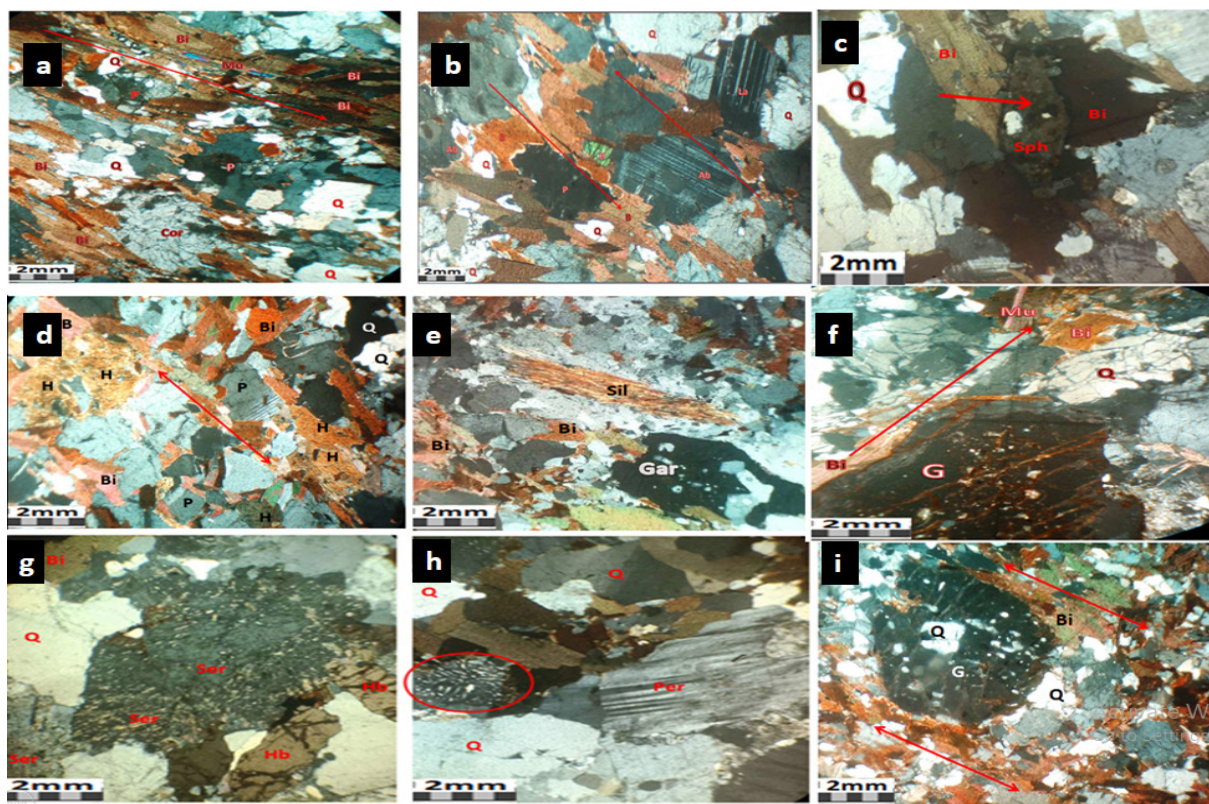


**Figure 4.** Photomicrograph of MBGn and GBS./**Figura 4.** Microfotografía de MBGn y GBS.

## Geochemistry

Twenty-eight (28) fresh representative samples consisting of twenty-two (22) migmatitic banded gneiss (MBGn) and Six (6) garnet-biotite schist (GBS) were selected for geochemical analyses.

## Analytical procedure

The samples were crushed in a jaw crusher at the Inorganic Geochemistry Research Laboratory of the Department of Geology, University of Nigeria, Nsukka. The crushed samples were pulverized in a Vibrating Disc Mill. Final size reduction, mixing and homogenization to  $< 75\mu\text{m}$  were done with a Mixer Mill. One hundred gram (100 g) of each sample were thereafter packaged and dispatched to Bureau Veritas Minerals Pty Ltd, Canning Vale, Perth, Western Australia for major element oxides and trace element geochemistry using X-Ray Fluorescence (XRF) and Inductively Coupled Mass

Spectrometer (ICP-MS), respectively. Details of the analytical procedure are in Ibe and Obiora (2019).

## Geochemical composition

### Major Elements

The major element oxides data and CIPW norms on the rocks are presented in Tables 2 and 3.

The gneisses (MBGn) have values of  $\text{SiO}_2$  in the range of 57.10 to 73.84% with a mean value of 67.44%. They contain moderate  $\text{Al}_2\text{O}_3$  (13.30-16.60%), low  $\text{TiO}_2$  (0.10- 1.15%),  $\text{MgO}$  (0.06-3.57%) and  $\text{MnO}$  (0.03- 0.14%) as well as high  $\text{K}_2\text{O}$  (0.95- 5.08%),  $\text{Na}_2\text{O}$  (2.18- 6.69%) and  $\text{CaO}$  (0.28- 8.26 %). The Fe-number (Total Fe) ranges from 3.96 to 13.4 with enrichment in alumina (12.3 to 17.1 %). The  $\text{TiO}_2/\text{Al}_2\text{O}_3$  ratio values of about 0.01-0.09, appear to be moderately high and have been given various interpretations. Goldschmidt (1954) reported that  $\text{TiO}_2/\text{Al}_2\text{O}_3$  ratio of about 0.04% is indicative of the presence of clayey components in

rocks while Spear and Kanaris-Sotirious (1976) suggested that the same ratio is indicative of sediments contaminated by basic to intermediate volcanic components. They are generally quartz, K-feldspar, albite, anorthite, hypersthene and corundum normative.

The schist (GBS) has moderate alumina to alkali ( $\text{Al}_2\text{O}_3/\text{K}_2\text{O}+\text{Na}_2\text{O}$ ) ratios (2.31 to 3.85 %), low  $\text{MgO}$  (3.56 to 5.91 %) and  $\text{CaO}$  (0.74 to 2.92 %) contents, with  $\text{MgO}$  exceeding  $\text{CaO}$ . Contents of  $\text{K}_2\text{O}$  are generally greater than those of  $\text{Na}_2\text{O}$  except in few cases (Table 3). The rocks plotted on the sedimentary field on the diagram of Tarney (1977) (Figure 5) which discriminates between sedimentary and igneous protoliths of metamorphic rocks.

Further discrimination of the sedimentary

protolith of the gneisses and schists was done by the plot of  $\log(\text{Fe}_2\text{O}_3^{(\text{t})}/\text{K}_2\text{O})$  vs  $\log(\text{SiO}_2/\text{Al}_2\text{O}_3)$  after Herron (1988) (Figure 6) was utilized.

The gneisses plot in the Fe-shale, Fe-sand and greywacke and arkose regions whereas the schists plot in the shale and greywacke regions. They plot on the continental field on the crustal discrimination diagram of Pearce *et al.* (1984) (Figure 7).

### Trace Elements

The trace elements compositions (ppm) of the rocks are presented in Table 4 and 5. Trace element distribution patterns for the migmatitic banded gneiss and garnet-mica schist from the study area have been normalized to

	<b>MBGn1</b>	<b>MBGn2</b>	<b>MBGn3</b>	<b>MBGn4</b>	<b>MBGn5</b>	<b>MBGn6</b>	<b>MBGn7</b>	<b>MBGn8</b>	<b>MBGn9</b>	<b>MBGn10</b>	<b>MBGn11</b>
<b>SiO<sub>2</sub></b>	66.19	67.56	61.93	73.84	65.55	57.10	66.10	65.73	67.09	69.69	67.52
<b>TiO<sub>2</sub></b>	1.15	0.41	0.42	0.24	0.44	0.84	0.47	0.55	0.47	0.30	0.37
<b>Al<sub>2</sub>O<sub>3</sub></b>	14.80	16.4	16.50	13.80	15.30	16.60	16.00	15.80	15.20	15.90	17.00
<b>Fe<sub>2</sub>O<sub>3</sub></b>	5.02	3.56	4.88	2.32	4.48	7.61	4.44	4.79	4.65	2.81	3.20
<b>FeO</b>	3.95	2.71	2.75	1.64	1.78	5.79	3.04	3.13	2.98	1.94	2.16
<b>MnO</b>	0.06	0.04	0.08	0.03	0.07	0.12	0.07	0.07	0.07	0.06	0.05
<b>MgO</b>	0.06	1.48	2.15	1.04	2.95	3.57	2.18	2.30	2.32	1.42	1.12
<b>CaO</b>	2.54	0.38	5.03	2.94	4.67	8.26	4.33	4.17	4.38	3.68	4.63
<b>Na<sub>2</sub>O</b>	3.01	4.62	4.42	3.75	3.89	2.41	3.82	3.62	3.67	6.69	4.06
<b>K<sub>2</sub>O</b>	5.08	1.82	1.42	1.24	2.11	1.73	1.92	2.27	1.61	0.95	1.10
<b>P<sub>2</sub>O<sub>5</sub></b>	0.45	0.19	0.17	0.12	0.18	0.23	0.15	0.20	0.18	0.12	0.14
<b>LOI</b>	0.37	0.36	0.34	0.27	0.34	1.03	0.37	0.41	0.24	0.34	0.46
<b>Total</b>	102.68	99.53	100.09	101.23	101.76	105.29	102.52	102.63	102.86	103.90	101.81
<b>A</b>	8.09	6.44	5.84	4.99	6.00	4.14	5.74	5.89	5.28	7.64	5.16
<b>Fe*</b>	8.97	6.27	7.63	3.96	6.26	13.40	7.48	7.92	7.63	4.75	5.36
<b>Log F/K</b>	-0.005	0.29	0.54	0.27	0.33	0.64	0.36	0.32	0.46	0.47	0.46
<b>S/A</b>	4.47	4.12	3.75	5.35	4.28	3.44	4.13	4.16	4.41	4.38	3.97
<b>Log S/A</b>	0.65	0.61	0.57	0.73	0.63	0.54	0.62	0.62	0.64	0.64	0.60
<b>P<sub>2</sub>O<sub>5</sub>/TiO<sub>2</sub></b>	0.39	0.46	0.39	0.52	0.39	0.27	0.32	0.37	0.38	0.39	0.38
<b>MgO/CaO</b>	0.02	3.89	0.43	0.35	0.63	0.43	0.50	0.55	0.53	0.39	0.24
<b>CIPW Norm values</b>											
<b>Q</b>	24.30	30.50	17.60	39.30	22.70	14.80	23.80	23.60	26.70	18.47	28.00
<b>Or</b>	29.80	10.70	8.30	7.30	12.40	10.20	11.30	13.30	9.50	5.60	6.50
<b>Ab</b>	25.20	38.80	37.00	31.50	32.60	20.17	32.00	30.30	30.80	56.10	34.10
<b>An</b>	9.60	0.70	20.90	13.74	18.00	29.20	20.40	19.30	20.20	10.50	21.96
<b>C</b>	0.80	6.60		1.24		8.00	0.13	0.30			1.10
<b>Di wo</b>	-	-	1.00	-	1.06	-	-	-	-	2.00	-

**Table 2: Continued**

	MBGn1	MBGn2	MBGn3	MBGn4	MBGn5	MBGn6	MBGn7	MBGn8	MBGn9	MBGn10	MBGn11
	MBGn12	MBGn13	MBGn14	MBGn15	MBGn16	MBGn17	MBGn18	MBGn19	MBGn20	MBGn21	MBGn22
Dien			1.23		2.00	8.10				3.50	
Hyen	15.0	51.0	4.70	3.33	5.90	8.10	6.70	6.70	6.70	18.0	3.60
mt	7.20	51.0	7.00	3.35	4.70	11.00	6.40	6.90	6.90	4.04	4.60
Il	22.0	08.0	08.0	0.45	0.80	1.60	0.90	1.04	0.90	0.60	0.70
he											
Ap	1.00	04.0	04.0	0.30	0.40	0.50	0.33	0.40	0.38	0.30	0.30
TiO <sub>2</sub>	0.45	0.99	0.86	0.97	0.10	0.20	0.44	0.38	0.84	0.96	0.14
	16.40	17.10	15.70	14.60	13.80	15.10	12.30	13.10	14.30	15.90	15.10
Fe <sub>2</sub> O <sub>3</sub>	3.98	7.99	6.89	7.53	1.45	1.92	4.18	3.36	6.42	7.26	1.90
FeO	3.04	4.65	5.04	2.84	0.21	0.23	1.83	1.36	4.65	5.78	1.33
MnO	0.10	0.14	0.13	0.14	0.05	0.05	0.07	0.05	0.12	0.14	0.06
MgO	14.2	3.26	3.02	3.29	3.34	0.54	0.37	0.29	2.32	0.22	0.46
CaO	3.08	12.8	18.8	1.75	0.79	1.84	1.92	2.02	2.59	2.90	1.67
Na <sub>2</sub> O	4.30	2.18	2.68	25.0	2.22	3.56	2.86	3.28	2.50	2.73	3.27
K <sub>2</sub> O	1.43	2.91	28.0	3.12	6.30	3.59	3.89	3.66	2.43	2.74	4.49
	0.13	0.76	0.18	0.12	0.08	0.09	0.09	0.07	0.20	0.21	0.08
LOI	0.32	11.0	0.85	0.73	0.38	0.32	0.05	0.03	0.56	0.47	0.28
Total	102.87	103.06	105.01	101.72	102.92	99.86	101.38	100.70	103.64	102.79	100.63
A	5.73	5.09	5.48	5.62	8.52	7.15	6.75	6.94	4.93	5.47	7.76
Fe*	7.02	12.64	11.93	10.37	1.66	2.15	6.01	4.72	11.07	13.04	3.23
Log F/K	0.44	0.44	0.39	0.38	-0.64	-0.27	0.03	-0.03	0.42	0.42	-0.37
S/A	4.16	3.61	4.14	4.44	5.38	4.80	5.97	5.58	4.67	3.99	4.78
Log S/A	0.62	0.56	0.62	0.65	0.73	0.68	0.78	0.75	0.67	0.60	0.68
P <sub>2</sub> O <sub>5</sub> /TiO <sub>2</sub>	0.30	0.77	0.21	0.12	0.79	0.47	0.21	0.19	0.24	0.21	0.60
MgO/CaO	0.46	2.55	1.61	1.88	4.22	0.29	0.19	0.14	0.90	0.08	0.28
CIPWNor											
Q	28.50	32.20	29.50	30.00	30.60	33.30	37.30	35.30	33.40	29.60	31.40
Or	84.0	17.10	16.50	18.30	37.00	21.10	22.90	21.50	14.30	16.11	26.40
Ab	36.07	18.30	22.50	20.90	18.60	29.80	24.00	27.50	21.00	22.90	27.40
An	14.35	14.0	81.0	7.90	3.40	85.0	9.00	9.50	11.50	13.00	7.72
C	25.0	10.00	5.30	4.20	2.10	2.20	0.12	0.24	3.30	3.70	2.00
Divo											
Dien											
Hyen	5.20	8.60	10.00	8.20	8.30	1.34	0.90	0.72	7.80	3.80	1.90
mt	5.80	11.60	10.00	6.80	0.60	0.30	4.80	3.40	9.30	10.50	2.70
Il	0.90	19.0	16.0	18.0	0.20	0.40	0.80	0.70	1.60	18.0	0.30
he						1.70	0.80	1.00			
ap	0.29	17.0	0.40	0.25	0.20	0.20	0.20	0.20	0.40	0.45	0.20

**Table 2.** Major element oxide (wt %) compositions and CIPW norm values of the gneisses around Njuakaku, southeast of Ogoja./**Tabla 2.** Composiciones de óxido de elemento principal (% en peso) y valores normativos CIPW de los gneises alrededor de Njuakaku, al sureste de Ogoja.

	<b>GBS1</b>	<b>GBS2</b>	<b>GBS3</b>	<b>GBS4</b>	<b>GBS5</b>	<b>GBS6</b>
<b>SiO<sub>2</sub></b>	61.05	62.71	60.86	60.67	57.09	65.16
<b>TiO<sub>2</sub></b>	0.90	0.87	0.94	0.96	1.14	0.80
<b>Al<sub>2</sub>O<sub>3</sub></b>	16.60	15.10	17.50	17.80	18.10	15.10
<b>Fe<sub>2</sub>O<sub>3</sub></b>	7.75	7.48	8.62	8.25	9.18	6.84
<b>FeO</b>	5.97	5.81	0.13	1.64	7.10	5.03
<b>MnO</b>	0.14	0.14	0.15	0.14	0.17	0.13
<b>MgO</b>	4.07	3.86	4.31	4.21	3.93	3.56
<b>CaO</b>	2.92	2.85	1.51	2.13	1.16	2.67
<b>Na<sub>2</sub>O</b>	2.84	2.77	1.90	3.42	2.01	2.62
<b>K<sub>2</sub>O</b>	2.78	2.62	2.64	2.52	3.69	2.41
<b>P<sub>2</sub>O<sub>5</sub></b>	0.20	0.21	0.19	0.22	0.16	0.19
<b>LOI</b>	0.45	0.40	1.18	0.62	1.01	0.46
<b>Total</b>	105.67	104.82	99.93	102.57	104.74	104.97
<b>A</b>	5.62	5.39	4.54	5.94	5.70	5.03
<b>Fe*</b>	13.72	13.29	8.75	9.89	16.28	11.87
<b>LogF/K</b>	0.44	0.45	0.51	0.52	0.39	0.45
<b>S/A</b>	3.67	4.15	3.47	3.40	3.15	4.31
<b>LogS/A</b>	0.56	0.61	0.54	0.53	0.49	0.63
<b>P<sub>2</sub>O<sub>5</sub>/TiO<sub>2</sub></b>	0.22	0.24	0.21	0.22	0.14	0.23
<b>MgO/CaO</b>	1.39	1.35	2.85	1.97	3.38	1.33
<b>CIPW Norm</b>						
<b>Q</b>	20.50	23.20	30.50	20.80	21.60	29.00
<b>Or</b>	16.30	15.40	15.50	14.80	21.70	14.20
<b>Ab</b>	23.80	23.20	15.90	28.70	16.80	22.00
<b>An</b>	13.10	12.70	6.21	9.10	4.70	12.00
<b>C</b>	4.10	3.00	9.20	6.10	9.00	3.80
<b>Di wo</b>						
<b>Di en</b>						
<b>Hy en</b>	13.40	12.90	8.60	10.40	13.60	11.30
<b>Ol</b>						
<b>mt</b>	11.20	10.80	0.60	2.90	13.20	9.90
<b>he</b>				6.20		
<b>ap</b>	0.40	0.50	0.40	0.50	0.40	0.40

**Table 3.** Major element oxide (wt %) compositions and CIPW norm values of the garnet biotite schist around Njuakaku, southeast of Ogoja./**Tabla 3.** Composiciones de óxido de elemento principal (% en peso) y valores normativos CIPW del esquisto de biotita granate alrededor de Njuakaku, al sureste de Ogoja.

chondrites after Thompson (1982) and plotted as spidergrams (Figure 8). They show an overall enrichment of the large ion lithophile elements (LILE: K, Ba and Rb) and depletion of the high field strength elements (HFSE:

Zr, Ti, Nb, Hf, Ta and Y). HFS concentrations are mainly controlled by the chemistry of the source and the crystal/melt processes that took place during the evolution of the rock.

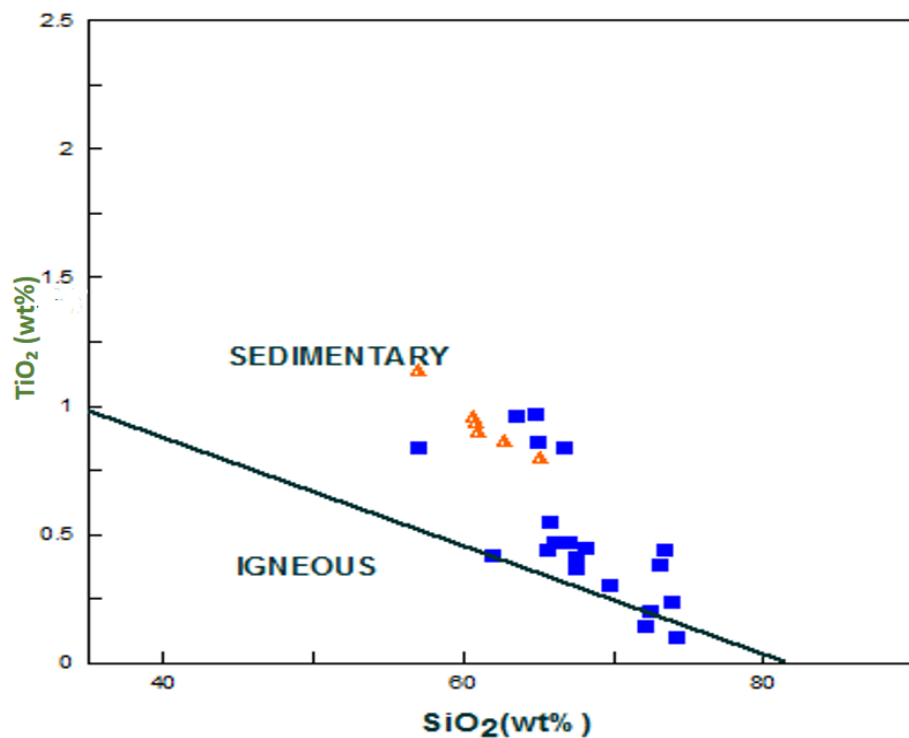


**Figure 5.** Bivariate ( $TiO_2$  versus  $SiO_2$ ) discrimination diagram./**Figura 5.** Diagrama de discriminación bivariante ( $TiO_2$  versus  $SiO_2$ ).

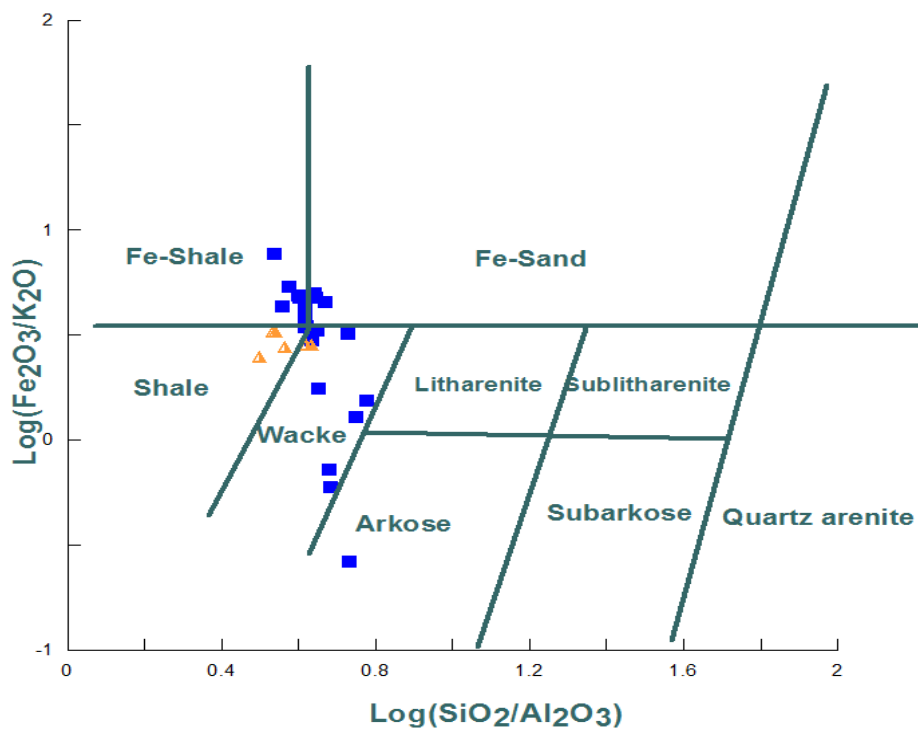


**Figure 6.** Plots of gneisses and schists on the  $\log(SiO_2/Al_2O_3)$  vs.  $\log(Fe_2O_3/t/K_2O)$  diagram for the discrimination of sedimentary protoliths./**Figura 6.** Gráficos de gneises y esquistos en el diagrama  $\log(SiO_2/Al_2O_3)$  vs.  $\log(Fe_2O_3/t/K_2O)$  para la discriminación de protolitos sedimentarios.

#### Rare-earth elements

The rare-earth elements compositions (ppm) of the rocks are presented in Table 6 and 7. Generally, the REE pattern for both the gneisses and schists display Light REE enrichment relative to Moderate REE and Heavy REE. The gneisses and the schists show light negative Eu anomaly. Whereas the gneisses show inclined

ses and schists display Light REE enrichment relative to Moderate REE and Heavy REE. The gneisses and the schists show light negative Eu anomaly. Whereas the gneisses show inclined

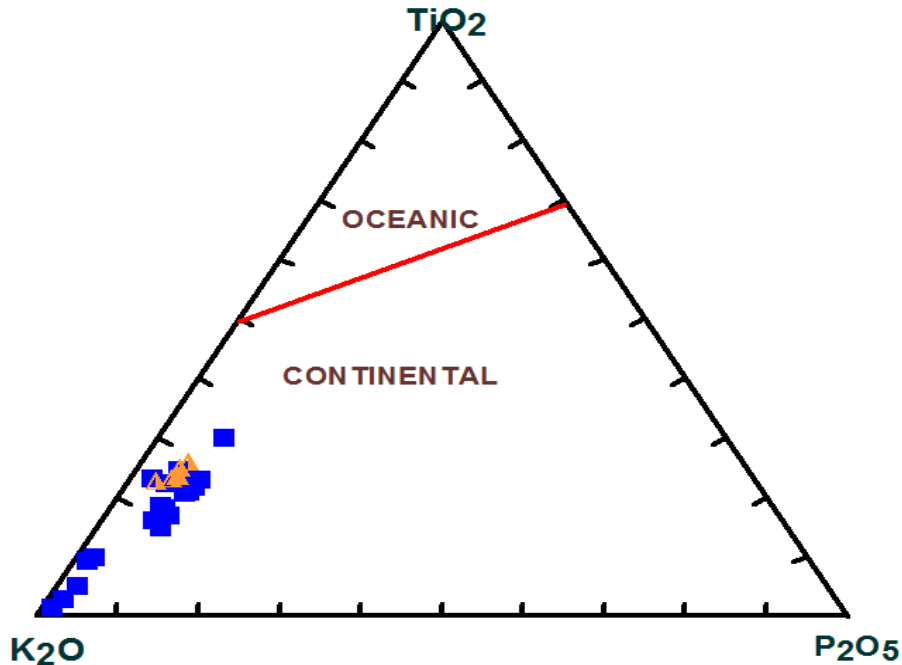


**Figure 7.** Ternary Plot of  $\text{K}_2\text{O}$ - $\text{TiO}_2$ - $\text{P}_2\text{O}_5$  showing continental discrimination of gneisses and schists./**Figura 7.** Gráfico ternario de  $\text{K}_2\text{O}$ - $\text{TiO}_2$ - $\text{P}_2\text{O}_5$  que muestra la discriminación continental de gneis y esquistos.

MREE and flat HREE, the schists show flat MREE and HREE (Figure 9). Specifically, the Eu-anomalies, expressed as  $(\text{Eu}/\text{Eu}^*)$  ranges from 0.02 to 1.4 in the gneisses and from 0.09 to 1.1 in the schist. The LaN/YbN ratios range from 7 to 93 for the gneisses and 1.9 to 46.4 for the schist.

#### Degree of alteration of the protoliths

Molar proportions of chemical index of alteration  $\text{CIA} = 100[\text{Al}_2\text{O}_3/(\text{Al}_2\text{O}_3 + \text{CaO}^* + \text{Na}_2\text{O} + \text{K}_2\text{O})]$  in molecular proportions where  $\text{CaO}^*$  is CaO in silicates only (Nesbitt and Young, 1982) was calculated. The CIA records the progressive alteration of potassium feldspars and plagioclase to clay minerals (Rahman and Suzuki, 2007). The index provides a means of ascertaining the extent or degree of weathering of the detritus constituting the protoliths. The values of CIA from the rocks range from 57.7-71.7 in the gneisses and 66.6-74.9 in the schists with mean of 68% and standard deviation of  $\pm 3.4$ . These values point to recycling processes and relatively moderate chemical wea-

thering of the protoliths. The samples show moderate weathering on the CIA versus  $\text{SiO}_2$  diagram of Nesbitt and Young (1982) and Taylor and McLennan (1985) (Figure 10).

#### Discussions

From field and petrographic studies, the study area is underlain by the rocks of the Nigerian Precambrian Basement Complex including (1) migmatitic banded gneiss, representing the Migmatite-Gneiss Complex or the Basement *sensu stricto* and (2) garnet-biotite schist representing the Schist belt. Minerals that make up the rocks include: quartz, K-feldspar (microcline), plagioclase, biotite, muscovite, chlorite, garnet, cordierite, sillimanite, sphene, zircon and opaques.

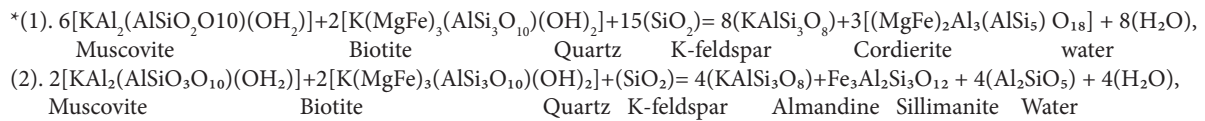
The assemblage of quartz + biotite + garnet + K-feldspar + oligoclase + cordierite + sphene + opaque in the migmatitic banded gneiss in the northern part of the study area is typical of the high-grade metamorphism, i.e. middle to upper amphibolite facies. According

to Bucher and Frey (1994), the index assemblage (garnet + biotite + plagioclase) has stability ranges of 550-600 °C and pressures of 3-10 Kb. The presence of K-feldspar in the absence of muscovite is expected at temperatures  $\geq$ 700-750 °C if  $\text{Al}_2\text{SiO}_5$  (kyanite or sillimanite) was present.

The mineral assemblage of migmatitic banded gneiss around Oku and Okundi, located in the western part of the study area represent middle to upper amphibolite facies conditions of metamorphism with temperatures of 600-700 °C and pressures of 3-10 Kb based on the stability of garnet (almandine) + biotite + cordierite + sillimanite. Howe-

ver, Massone and Schreyer (1987) stated that the presence of K-feldspar and plagioclase might be indicative of the fact that the conditions reached the upper amphibolite facies metamorphism, 670-700 °C. According to Ugwuonah and Obiora (2011), the index minerals could have been formed through the following reactions:<sup>\*</sup>

The characteristic mineral assemblage of the garnet-biotite schist in the study area which includes biotite, plagioclase (An<sub>39</sub>) and garnet suggests high grade regional metamorphism corresponding to middle amphibolite facies. The growth of garnet with inclusions



	<b>MBGn1</b>	<b>MBGn2</b>	<b>MBGn3</b>	<b>MBGn4</b>	<b>MBGn5</b>	<b>MBGn6</b>	<b>MBGn7</b>	<b>MBGn8</b>	<b>MBGn9</b>	<b>MBGn10</b>	<b>MBGn11</b>
<b>Sc</b>	6.9	6.1	9.8	2.9	10.2	18.5	12.4	8.6	11	6.4	3.5
<b>V</b>	36.7	45.3	79.6	27.7	72.8	123	76.8	80.3	75	46.9	44
<b>Cr</b>	14	24	39	13	91	124	43	52	50	38	14
<b>Co</b>	18.5	17.5	18.9	12.2	20.8	26.9	15.8	20.5	24.5	25.2	10.9
<b>Ni</b>	12	20	22	10	62	64	20	26	30	26	8
<b>Cu</b>	18	18	6	14	12	54	4	10	4	14	22
<b>Zn</b>	125	60	60	35	50	100	50	50	60	40	40
<b>Ga</b>	21.8	21.3	19.7	13.3	17.4	22.2	18.4	18.6	17.8	22.2	20.8
<b>Rb</b>	238	102	48.6	43.9	83	91.4	69.4	79.9	51.2	32.2	35.2
<b>Sr</b>	334	608	578	469	511	444	450	401	430	692	685
<b>Y</b>	32.4	8.6	11.1	6.28	15.5	34.5	12.2	12.3	13.6	8.12	8.08
<b>Zr</b>	890	150	118	94	176	214	121	199	113	130	171
<b>Nb</b>	40.3	6.47	3.59	7.01	4.61	16.2	4.24	3.75	4.02	3.53	1.53
<b>Sn</b>	1.4	1.6	1.6	0.8	1.4	4.8	1.4	1.2	1.4	0.8	0.8
<b>Sb</b>	0.5	0	0.6	0.4	0.3	0.4	0.2	0.2	1.1	1.1	0.1
<b>Cs</b>	0.84	1.46	0.41	1.12	2.05	3.52	1.89	1.79	1.66	0.9	0.63
<b>Ba</b>	1670	430	512	358	635	504	636	818	489	494	346
<b>Hf</b>	22.2	3.4	2.81	2.33	4.14	5.32	5.2	5.73	3.25	2.88	4.72
<b>Ta</b>	3.07	0.6	0.38	0.33	0.45	1.22	0.34	0.36	0.35	0.58	0.09
<b>W</b>	216	203	144	122	140	90.4	90.8	91.7	150	220	68.4
<b>Tl</b>	1.2	0.6	0.4	0.4	0.4	0.6	0.4	0.4	0.4	0.2	0.4
<b>Pb</b>	27	12	8	8	9	10	9	9	5	9	6
<b>Th</b>	68.4	3.12	1.79	3.52	8.08	12	5.68	5.81	3.79	1.97	0.38
<b>U</b>	2.4	0.84	0.08	0.23	0.54	2.93	0.63	1.19	0.65	0.29	0.23
<b>Ga</b>	21.8	21.3	19.7	13.3	17.7	22.2	18.4	18.6	16.7	22.2	20.8
<b>Y+Nb</b>	72.7	15.07	14.69	13.29	20.11	50.7	16.44	16.05	17.62	11.65	9.61

**Table 4:** Continued

	<b>MBGn12</b>	<b>MBGn13</b>	<b>MBGn14</b>	<b>MBGn15</b>	<b>MBGn16</b>	<b>MBGn17</b>	<b>MBGn18</b>	<b>MBGn19</b>	<b>MBGn20</b>	<b>MBGn21</b>	<b>MBGn22</b>
<b>Sc</b>	12.2	18.4	16.2	19.2	3.7	4.4	5.7	5.1	12.6	16.3	3.4
<b>V</b>	49	146	128	151	6.9	10.6	12.2	13.4	122	137	9.8
<b>Cr</b>	30	127	115	120	3	3	3	7	93	111	1
<b>Co</b>	18	23.9	33	25.8	25.5	24.5	14.9	16.8	24.5	29.2	17.5
<b>Ni</b>	28	98	70	68	4	4	1	4	58	68	6
<b>Cu</b>	94	80	28	44	8	6	18	16	44	24	8
<b>Zn</b>	40	120	90	110	25	40	65	70	55	80	30
<b>Ga</b>	17.2	24	17.5	18.8	11.5	15.3	13.3	14.9	16.2	17.3	15.3
<b>Rb</b>	38.7	136	95.7	120	119	84.3	43	39.8	79.6	82.9	98.9
<b>Sr</b>	681	165	213	200	187	196	174	190	181	199	207
<b>Y</b>	21.6	29.5	33	28.1	7.78	12.3	52.5	35.8	33.2	34.2	11
<b>Zr</b>	275	240	209	197	71.5	264	688	514	193	225	144
<b>Nb</b>	6.11	14.6	10.1	13.9	1.99	3.49	9.64	9.44	11.2	11.7	2.44
<b>Sn</b>	1.4	1.4	2	1.8	1	0.8	0.8	1	2.2	2.4	1.2
<b>Sb</b>	0.3	0.3	0.1	0.2	0.2	0.3	0.1	0.2	0.1	0.3	0.3
<b>Cs</b>	1.94	4.3	4.69	5.89	1.42	1.54	0.28	0.23	4.24	5.07	1.39
<b>Ba</b>	697	849	552	660	1410	791	2470	2200	492	522	1080
<b>Hf</b>	7.36	6.93	6.02	5.73	2.25	7.7	15.9	11.5	5.02	5.92	4.48
<b>Ta</b>	0.51	0.8	0.83	0.95	0.82	0.46	0.47	0.47	0.9	0.96	0.34
<b>W</b>	170	53.6	235	82.2	530	236	180	186	96.1	121	189
<b>Tl</b>	0.2	0.8	0.6	0.8	0.8	0.6	0.2	0.2	0.6	0.6	0.8
<b>Pb</b>	27	18	17	16	44	34	6	6	15	16	41
<b>Th</b>	14.2	18.1	8.25	7.66	10.1	55	8.46	4.59	8.63	8.1	25.4
<b>U</b>	2.95	2.85	2.11	2.46	1.42	5.66	1	0.42	2.34	2.84	3.02
<b>Ga</b>	17.2	24	17.8	18.8	11.5	15.3	13.3	14.9	16.2	17.3	15.3
<b>Y+Nb</b>	27.71	44.1	43.1	42	9.77	15.79	62.14	45.24	44.4	45.9	13.44

**Table 4.** Trace elements compositions (ppm) of the gneisses around Njuakaku, southeast of Ogoja./**Tabla 4.** Composiciones de oligoelementos (ppm) de los gneis alrededor de Njuakaku, al sureste de Ogoja.

of muscovite, biotite and quartz and the garnet surrounded by the crystals of biotite and quartz are some of the microstructures indicating prograde metamorphism while the sericitization of plagioclase crystals and the myrmekitic structures are indicative of retrograde metamorphism. Alterations by sericitization, together with the myrmekitic intergrowths in the gneisses suggest that retrograde metamorphism was superimposed on these high-grade amphibolite facies rocks (Ugwuonah *et al.*, 2017).

Myrmekitic intergrowth is commonly associated with the breakdown of feldspars in gneisses and indicative of retrograde metamorphism (Ugwuonah *et al.*, 2017).

As observed in this study, biotite and quartz showed considerable variations in

their sizes; also, different grains of plagioclase showed different compositions which were also obvious in their different anorthite compositions. This may be indicative of a metasedimentary origin for the rocks (Obiora, 2006). The presence of almandine garnet in the migmatitic banded gneisses and the garnet-biotite schists confirms a pelitic sedimentary origin for the rocks.

On a  $\text{TiO}_2$  versus  $\text{SiO}_2$  diagram of Tarnay (1977), the gneisses and the schists dominantly plot in sedimentary field (Figure 6).

The plot of  $\log(\text{Fe}_2\text{O}_3^{(\text{t})}/\text{K}_2\text{O})$  vs  $\log(\text{SiO}_2/\text{Al}_2\text{O}_3)$  after Herron (1988) shows that the protoliths of the gneisses are predominantly Fe-shale, Fe-sand and greywacke and arkose while those of the schists are shales and greywackes.

	<b>GBS1</b>	<b>GBS2</b>	<b>GBS3</b>	<b>GBS4</b>	<b>GBS5</b>	<b>GBS6</b>
<b>Sc</b>	21.5	19.4	22.7	22.9	26.4	18.8
<b>V</b>	168	149	179	173	173	137
<b>Cr</b>	126	111	120	120	161	102
<b>Co</b>	30.2	26.2	36.3	29.4	27.9	29
<b>Ni</b>	80	76	90	90	88	68
<b>Cu</b>	12	8	114	58	46	10
<b>Zn</b>	120	105	130	115	130	95
<b>Ga</b>	20.8	18.1	21.3	21.1	24.5	16.4
<b>Rb</b>	92.9	85.6	88.1	82.2	137	80.8
<b>Sr</b>	224	217	156	168	235	211
<b>Y</b>	36.2	36.2	37.1	38.5	37.2	31.3
<b>Zr</b>	189	176	194	201	230	163
<b>Nb</b>	9.7	9.6	9.21	9.99	16.1	8.17
<b>Sn</b>	2.6	2.2	1.6	1.6	2.6	2
<b>Sb</b>	0.2	0.2	0.3	0.3	0	0.4
<b>Cs</b>	5.23	5.04	4.64	4.49	6.7	4.52
<b>Ba</b>	548	528	526	468	767	479
<b>Hf</b>	4.95	4.67	5.05	5.94	6.64	4.25
<b>Ta</b>	0.84	0.87	0.89	0.8	1.11	0.7
<b>W</b>	161	134	175	126	51	154
<b>Tl</b>	0.6	0.4	0.6	0.6	0.8	0.4
<b>Pb</b>	18	17	12	13	18	16
<b>Th</b>	7.07	7.45	8.12	8.73	9.23	6.16
<b>U</b>	2.13	2.65	2.86	2.7	3.29	1.93
<b>Ga</b>	20.8	18.1	21.3	21.1	24.5	16.4
<b>Y+Nb</b>	45.9	45.8	46.31	48.49	53.3	39.47

**Table 5.** Trace elements compositions (ppm) of the garnet biotite schist around Njuakaku, southeast of Ogoja./**Tabla 5.** Composiciones de oligoelementos (ppm) del esquisto de biotita granate alrededor de Njuakaku, al sureste de Ogoja.

The  $\text{TiO}_2/\text{Al}_2\text{O}_3$  ratio of the migmatitic rocks points towards a mixed nature of the parent rocks which are predominantly made up of greywacke, shales with subordinate basic to intermediate volcanic components as deduced from the geochemical character of the rocks.

Truswell and Cope (1963), McCurry (1976), Ajibade *et al.* (1979), Holt (1982), Obiora (2006) and Danbatta (2008) had established sedimentary protoliths for the metamorphic rocks in the Nigerian Precambrian Basement Complex. However, there are contrasting views concerning the evolution of the gneisses. Some authors believe that the gneisses are

of igneous protolith while others noted that some gneisses evolved from partial melting of pre-existing metasediments (McCurry, 1971; Obiora, 2012). The overall geochemical data of the schists and gneisses suggests that their sedimentary progenitors were derived from a cratonic source (Taylor and McLennan, 1985; Das *et al.*, 2008).

## Conclusion

The assemblage of the migmatitic banded gneiss around the northern, western and central parts of the study area is typical of mi-

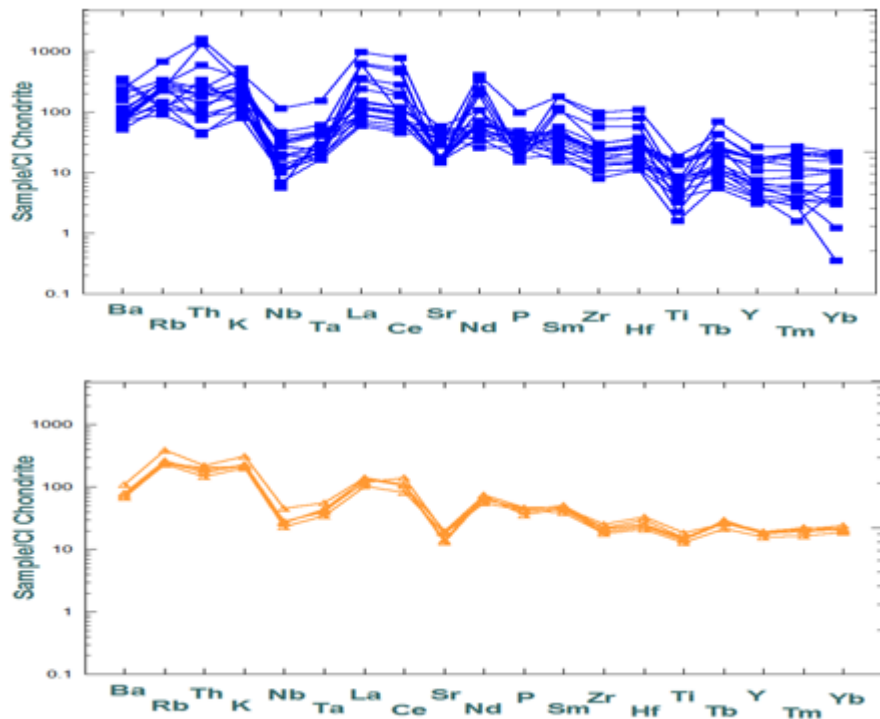


**Figure 8.** Chondrite-normalized Spidergram for MBGn and GBS./**Figura 8.** Spidergram normalizado con condritas para MBGn y GBS.

ddle to upper amphibolite facies with stability ranges of 550-700 °C and pressures of 3-10 Kb. The characteristic mineral assemblage of the garnet-biotite schist in the eastern part of the study area suggests high grade regional metamorphism corresponding to the middle amphibolite facies. Although several theories have emerged as to the origin of myrmekite in metamorphic rocks, the alterations by sericitization together with the myrmekitic intergrowths in the gneisses could mean that retrograde metamorphism was superimposed on these high-grade amphibolite facies rocks. The gneisses were confirmed to be derived from shale, greywackes and arkosic sands while the schists were derived from shales and greywackes. The CIA values point to recycling processes and relatively moderate chemical weathering of the protoliths. The overall geochemical data of the schists and gneisses suggests that their sedimentary progenitors were derived from a cratonic source. This result is consistent with other parts of the Nigerian Precambrian Basement complex.

## Acknowledgements

The assistance of the Association of Applied Geochemists (AAG) in carrying out the whole rock geochemical analyses (In-Kind Analytical support-student initiative program) is greatly acknowledged. The author is grateful to Theophilus Clavell Davies for securing the TETFund ((TETFUND/DESS/UNI/NSUKKA/2017/RP/VOL.I)) which was used for the field work and petrographic studies and also to Smart Chika Obiora for proof reading the thesis which the work was extracted from.

## References

- Ajibade, A.C., Fitches, W.R. and Wright, J.B. 1979. The Zungeru Milonites, Nigeria: recognition of Major tectonic unit. *Revue de Géologie Géographie Physique*, 21: 359–363.
- Annor, A.E. 1998. Structural and chronological relationship between the low-grade Igarra schist and its adjoining Okene migmatite-gneiss terrain in the Precambrian exposure of southwestern Nigeria. *Journal of Mining Geology*, 34 (2): 187-196.

	<b>MBGn1</b>	<b>MBGn2</b>	<b>MBGn3</b>	<b>MBGn4</b>	<b>MBGn5</b>	<b>MBGn6</b>	<b>MBGn7</b>	<b>MBGn8</b>	<b>MBGn9</b>	<b>MBGn10</b>	<b>MBGn11</b>
<b>La</b>	231	21.9	15.6	14.1	36.3	34.5	18.5	21.5	22.5	17.5	8.17
<b>Ce</b>	479	45.5	32.2	28.1	73.6	71.2	41.2	46.1	44.1	37	17.4
<b>Pr</b>	55.9	5.79	55.2	3.36	8.55	8.54	4.6	5.07	5.91	4.81	2.19
<b>Nd</b>	191	21.4	15.8	12.1	31.2	31.8	17.3	18.8	23.9	21.4	9.77
<b>Sm</b>	27.70	4.6	2.95	2.36	5.36	6.53	3.23	3.23	4.13	3.72	2.2
<b>Eu</b>	2.08	1.04	0.97	0.63	1.19	1.29	1	0.9	0.98	1.34	0.56
<b>Gd</b>	12.60	3.32	2.44	1.34	3.28	5.6	2.52	2.16	2.9	2.24	1.73
<b>Tb</b>	1.63	0.41	0.37	0.21	0.51	0.91	0.42	0.43	0.43	0.3	0.3
<b>Dy</b>	6.34	1.87	2.2	1.16	2.82	5.93	0	2.2	2.28	1.31	1.52
<b>Ho</b>	1.11	0.3	0.34	0.22	0.54	1.23	0.13	0.35	0.51	0.43	0.39
<b>Er</b>	2.88	0.78	1.26	0.59	1.34	3.18	0.54	1.18	1.25	0.67	0.81
<b>Tm</b>	0.32	0.09	0.1	0.09	0.22	0.52	0.20	0.16	0.14	0.04	0.09
<b>Yb</b>	1.78	0.52	0.21	1.37	1.76	3.65	0.15	1.06	0.52	0.86	0.32
<b>Lu</b>	0.22	0.04	0.12	0.07	0.2	0.54	0.13	0.16	0.19	0.12	0.07
<b><math>\Sigma</math>REE</b>	1013.56	107.56	129.76	65.7	166.87	175.42	89.92	103.3	109.74	91.74	45.52
<b><math>\Sigma</math>LREE</b>	984.6	99.19	121.75	60.02	155.01	152.57	84.83	94.7	100.54	84.43	39.73
<b><math>\Sigma</math>HREE</b>	26.88	7.33	7.04	5.05	10.67	21.56	4.09	7.7	8.22	5.97	5.23
<b><math>\Sigma</math>LREE/HREE</b>	36.62	13.53	17.29	11.88	14.52	7.07	20.74	12.29	12.23	14.14	7.59
<b>La<sub>N</sub>/Yb<sub>N</sub></b>	93.08	30.20	53.28	7.38	14.79	6.77	88.46	14.54	31.03	14.59	18.31
<b>Ce<sub>N</sub>/Yb<sub>N</sub></b>	74.75	24.30	42.59	5.69	11.61	5.41	76.29	12.08	23.55	11.95	15.10
<b>La<sub>N</sub>/Sm<sub>N</sub></b>	5.38	3.07	3.41	3.85	4.37	3.41	3.69	4.29	3.51	3.03	2.39
<b>La<sub>N</sub>/Lu<sub>N</sub></b>	112.53	58.67	13.93	21.58	19.45	6.84	15.25	14.40	12.69	15.62	12.50
<b>Eu/Eu*</b>	0.34	0.81	1.10	1.08	0.86	0.65	1.07	1.04	0.86	1.41	0.87
	<b>MBGn12</b>	<b>MBGn13</b>	<b>MBGn14</b>	<b>MBGn15</b>	<b>MBGn16</b>	<b>MBGn17</b>	<b>MBGn18</b>	<b>MBGn19</b>	<b>MBGn20</b>	<b>MBGn21</b>	<b>MBGn22</b>
<b>La</b>	57.8	46.7	29.6	26.5	21.2	144	152	86.4	28.1	150	82.8
<b>Ce</b>	114	93.2	61.6	54.4	43	277	317	172	58.5	58.4	123
<b>Pr</b>	14	11.5	7.79	6.66	5.11	32.6	40.2	22.7	7.38	7.67	14
<b>Nd</b>	50.6	42.2	33.3	28	17.3	112	157	91	28.5	30.3	50.4
<b>Sm</b>	8.81	8.44	6.88	6.2	3.03	18.1	27.5	16.1	5.93	7.1	8.79
<b>Eu</b>	1.99	1.23	1.62	1.15	0.92	1.32	0.17	2.64	1.47	1.36	1.16
<b>Gd</b>	5.4	6.12	5.84	4.75	1.84	9.97	18.6	12.8	5.08	5.83	4.79
<b>Tb</b>	0.82	0.88	0.99	0.71	0.24	1.09	2.64	1.6	0.89	1.01	0.58
<b>Dy</b>	4.25	5.2	5.91	4.8	1.64	3.84	1.16	8.76	5.05	5.83	2.4
<b>Ho</b>	0.81	1.08	1.14	1	0.25	0.43	2.12	1.88	1.14	1.19	0.4
<b>Er</b>	1.88	3.27	3.36	2.7	0.64	0.76	5.27	5.71	3.03	3.23	1.04
<b>Tm</b>	0.28	0.52	0.55	0.5	0.07	0.09	0.69	0.41	0.53	0.55	0.13
<b>Yb</b>	1.77	3.27	3.31	3.07	0.06	0.61	3.71	2.6	2.85	3.49	0.8
<b>Lu</b>	0.56	0.63	0.44	0.09	0.08	0.64	0.34	0.41	0.47	0.86	0.79
<b><math>\Sigma</math>REE</b>	262.97	224.24	162.33	140.53	95.38	602.45	728.4	425.01	148.92	276.82	291.08
<b><math>\Sigma</math>LREE</b>	245.21	202.04	139.17	121.76	89.64	583.7	693.7	388.2	128.41	253.47	278.99
<b><math>\Sigma</math>HREE</b>	15.77	20.97	21.54	17.62	4.82	17.43	34.53	34.17	19.04	21.99	10.93
<b><math>\Sigma</math>LREE/HREE</b>	15.54	9.63	6.46	6.91	18.59	33.48	20.08	11.36	6.74	11.52	25.52
<b>La<sub>N</sub>/Yb<sub>N</sub></b>	23.42	10.24	6.41	6.19	253.44	169.32	29.38	23.83	7.07	30.82	74.24
<b>Ce<sub>N</sub>/Yb<sub>N</sub></b>	17.89	7.91	5.16	4.92	199.07	126.13	23.73	18.37	5.70	4.64	42.70
<b>La<sub>N</sub>/Sm<sub>N</sub></b>	4.23	3.57	2.77	2.75	4.51	5.13	3.56	3.46	3.05	13.63	6.08
<b>La<sub>N</sub>/Lu<sub>N</sub></b>	11.06	7.94	7.20	31.55	28.40	24.11	47.91	22.58	6.40	18.69	11.23
<b>Eu/Eu*</b>	0.88	0.52	0.81	0.64	1.19	0.30	0.02	0.56	0.81	0.64	0.54

**Table 6.** Rare-earth elements compositions (ppm) of the gneisses around Njuakaku, southeast of Ogoja./**Tabla 6.** Composiciones de elementos de tierras raras (ppm) de los gneis alrededor de Njuakaku, al sureste de Ogoja.

Bucher, K. and Frey, M. 1994. Petrogenesis of Metamorphic rocks. Springer Verlag, Berlin, 318 p.  
 Burke, K.C. and Dewey, J.F. 1972. Orogeny in Africa. In:

Dessauvagie TFJ, Whiteman A.J. (eds), *Africa geology*. University of Ibadan Press, Ibadan: 583–608.  
 Das, B. K., Gaye, B. and Kaur, P. 2008. Geochemistry

	<b>GBS1</b>	<b>GBS2</b>	<b>GBS3</b>	<b>GBS4</b>	<b>GBS5</b>	<b>GBS6</b>
<b>La</b>	28.7	27.8	32	33.8	33.6	24.1
<b>Ce</b>	7.4	86.8	64.8	66.8	66.4	50.5
<b>Pr</b>	7.77	7.31	8.31	9.05	8.77	6.12
<b>Nd</b>	30.5	29.5	31.1	35.2	34.1	26.4
<b>Sm</b>	6.65	6.6	7.85	7.12	7.09	5.96
<b>Eu</b>	1.36	1.37	1.48	1.27	1.55	1.33
<b>Gd</b>	5.05	6.09	6.12	6.48	5.93	5.01
<b>Tb</b>	1	1.1	1.02	1.04	0.98	0.81
<b>Dy</b>	6.04	6.04	6.33	6.08	6.1	5.64
<b>Ho</b>	1.26	1.27	1.4	1.37	1.33	1.22
<b>Er</b>	3.74	3.4	3.46	3.62	3.67	2.96
<b>Tm</b>	0.58	0.49	0.53	0.56	0.54	0.42
<b>Yb</b>	3.39	3.56	3.48	3.71	4.09	3.23
<b>Lu</b>	0.54	0.46	0.36	0.54	0.45	0.45
<b>ΣREE</b>	103.98	181.79	168.24	176.64	174.6	134.15
<b>ΣLREE</b>	81.02	158.01	144.06	151.97	149.96	113.08
<b>ΣHREE</b>	21.6	22.41	22.7	23.4	23.09	19.74
<b>ΣLREE/HREE</b>	3.75	7.05	6.34	6.49	6.49	5.72
<b>La<sub>N</sub>/Yb<sub>N</sub></b>	6.07	5.60	46.39	6.53	5.89	5.35
<b>Ce<sub>N</sub>/Yb<sub>N</sub></b>	0.60	6.77	33.92	5.00	4.50	4.34
<b>La<sub>N</sub>/Sm<sub>N</sub></b>	2.78	2.71	3.81	3.06	3.05	2.61
<b>La<sub>N</sub>/Lu<sub>N</sub></b>	5.69	6.47	6.26	6.70	8.00	5.73
<b>Eu/Eu*</b>	0.71	0.66	1.18	0.57	0.73	0.74

**Table 7.** Rare-earth elements compositions (ppm) of the schist from the Bamenda massif./**Tabla 7.** Composiciones de tierras raras (ppm) del esquisto del macizo de Bamenda.

#### Key Abbreviations

A= Na20+k20 (alkali); Fe\*=Total iron; F/K=Fe2O3/ k20; S/A= SiO2/ Na20+k20 (alkali); Q= Quartz; Or= Orthoclase; Ab= Albite; An= Anorthite; C= Corundum; Di= Diopside; Hy=Hypersthene; En= Enstatite; Ol= Olivine; mt= magnetite; He=Hematite; Il= Ilmenite; Ap= Apatite; CIPW= Cross, Iddings, Pearson and Washington

- of Renuka Lake and wetland sediments, Lesser Himalaya (India): implications for source-area weathering, provenance and tectonic setting. *Environmental Geology*, 54: 137–163.
- Danbatta, U.A. 2008. Precambrian crustal development in the northwestern part of Zuru schist belt, northwestern Nigeria. *Journal of Mining and Geology*, 44 (1): 45–56.
- Goldschmidt, V.M. 1954. Geochemistry. Clarendon Press, Oxford. 730 p
- Herron, M. M. 1988. Geochemical classification of terrigenous sands and shales from core or log data. *Journal of Sedimentary Petrology*, 58: 820–829.
- Holt, R.W. 1982. The Geotectonic evolution of the Anka Belt in the Precambrian Basement Complex of Northwestern Nigeria. [Unpublished. Ph.D. Thesis], the Open University, Milton Keynes, England: 264 p.
- Ibe, C.U and Obiora, S.C. 2019. Geochemical characterization of Granitoids in Katchuan Irruan area: further evidence for peraluminous and shoshonitic compositions and post-collisional setting of granitic rocks in the Precambrian Basement Complex of Nigeria. *Acta Geochimica*, 38(5): 734–752.
- Kinnaird, J.A. 1984. Contrasting styles of Sn-Nb-Ta-Zn mineralization in Nigeria. *Journal of African Earth Sciences*, 2: 81–90.
- Kroner, A., Ekwueme B.N and Pidgeon R.T. 2001. The oldest rocks in West Africa: SHRIMP Zircon age for early Archean migmatitic orthogneiss at Kaduna, Northern Nigeria. *Journal of Geology*, 109(3): 399–406.

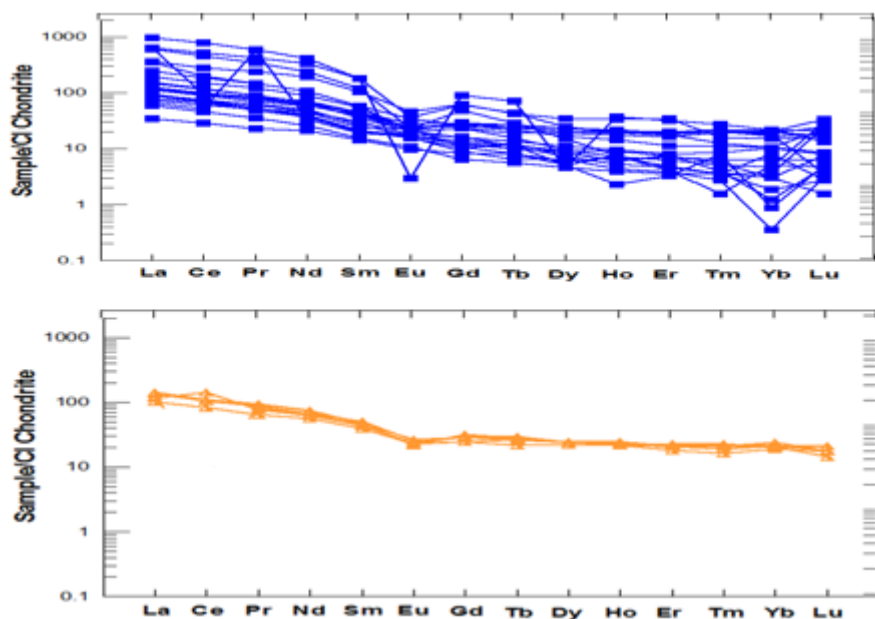


**Figure 9.** Chondrite-normalized REE diagrams for MBGn and GBS./**Figura 9.** Diagramas REE normalizados con condrita para MBGn y GBS.

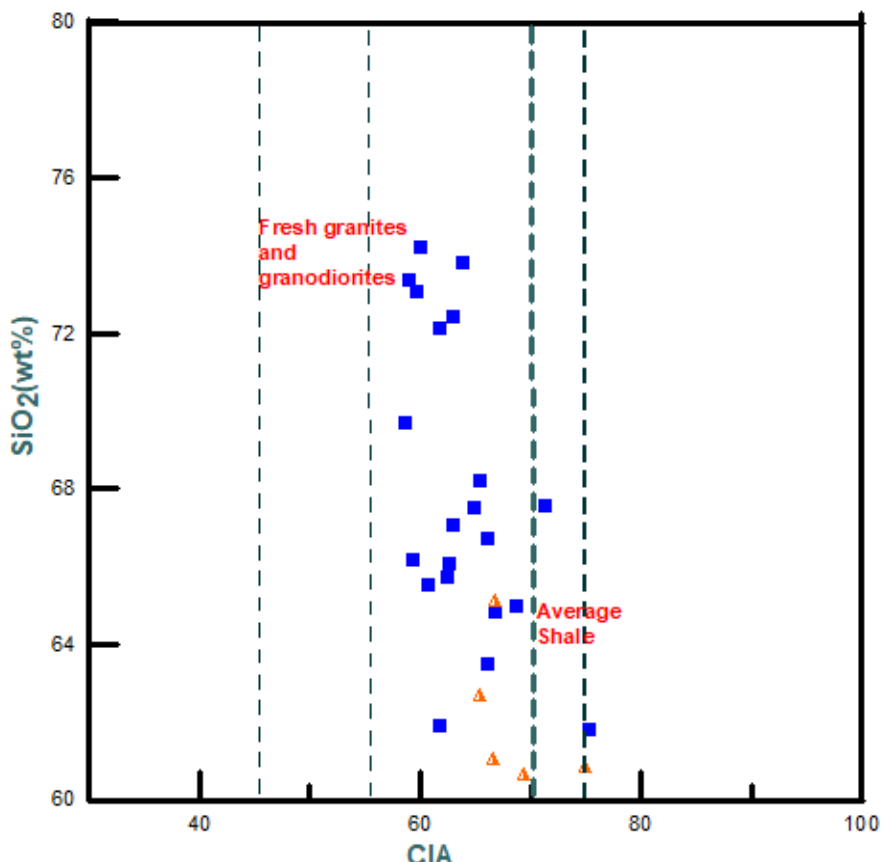


**Figure 10.** CIA (Chemical Index of Alteration) versus  $\text{SiO}_2$ ./**Figura 10.** CIA (índice químico de alteración) versus  $\text{SiO}_2$ .

- Liégeois, J.P., Abdelsalam, M.G., Ennih, N. and Ouabadi, A. 2013. Metacraton: Nature, genesis and behavior. *Gondwana Research*, 23: 220-237.  
 Massone, H.J. and Shreyer, W. 1987. Phengite Geobarrowmetry based on the limiting assemblage with

- K-feldspar, Phlogopite and Quartz. *Contribution to Mineralogy and petrology*, 96: 212–224.  
 McCurry, P. 1971. Pan-African Orogeny in Northern Nigeria: *Geological Society of America Bulletin*, 82: 3251-3263.

- McCurry, P. 1976. The geology of the Precambrian to lower Paleozoic rocks of Nigeria. In: Kogbe, C.A. (ed.), *Geology of Nigeria*. Elizaberthan, Lagos, Nigeria. 15-31.
- Nigerian Geological Survey Agency (NGSA), 2011. Geological Map of Nigeria.
- Nesbitt, H.W and Young, G.M. 1982. Early Proterozoic climates and plate motions inferred from major element chemistry of lutites. *Nature*, 299: 715-717.
- Obiora, S.C. 2006. Petrology and geotectonic setting of the Basement Complex rocks around Ogoja, Southeastern Nigeria. *Ghana Journal of Science*, 46: 13-46.
- Obiora, S.C. 2012. Chemical characterization and tectonic evolution of hornblende-biotite granitoids from the Precambrian Basement Complex around Ityowanye and Katsina-Ala, Southeastern Nigeria. *Journal of Mining and Geology*, 48(1): 13-29.
- Pearce, J.A., Harris, N.B.W., Tindle, A.G. 1984. Trace element discrimination diagram for the tectonic interpretation of granitic rocks. *Journal of Petrology*, 25 (4): 956-983.
- Rahman J. and Suzuki S. 2007. Geochemistry of sandstone from the Miocene Surma group, Bengal basin, Bangladesh: Implications for provenance, tectonic setting and weathering. *Geochemical Journal*, 41(6): 415-428.
- Spears, D.A and Kanaris-Sotirious, R. 1976. Titanium in some carboniferous sediment from Great Britain. *Geochimica et Cosmochimica acta*, 40: 345-351.
- Sun, S.S., and McDonough, W.F. 1991. Chemical and isotopic systematic of oceanic basalts: implication for mantle composition and processes. In: Saunders, A.D., Norry, M.J. (eds.), *Magmatic in Oceanic Basins*. Geology Society of London, Special Publication, 42, 313–345.
- Tarney, J. 1977. Petrology, mineralogy and geochemistry of the Falkland Plateau basement Rocks, site 330, Initial reports-deep sea drilling project, 36: 893-921.
- Taylor, S.R., and McLennan, S.M. 1985. Continental Crust: its Composition and Evolution. *Blackwell Scientific Publications*, Oxford, 311pp.
- Thompson R.N. 1982. British Tertiary volcanic province. *Scottish Journal of Geology*, 18: 49-67.
- Truswell, J.F. and Cope, R.N. 1963. The Geology of parts of Niger and Zaria Provinces, Northern Nigeria: *Geological Survey Nigeria Bulletin*, 29: 52.
- Ugwuonah E.N., and Obiora, S.C. 2011. Geothermometric and geobarometric signatures of metamorphism in the Precambrian basement complex rocks around Keffi, north-central Nigeria. *Ghana Journal of Science*, 51: 73-87.
- Ugwuonah E.N., Tsunogae, T., and Obiora, S.C. 2017. Metamorphic P-T evolution of garnet staurolite-biotite pelitic schist and amphibolites from Keffi, north central Nigeria: Geothermobarometry, mineral equilibrium modeling and P-T path. *Journal of African Earth Sciences*, 129: 1-16.

**Recibido:** 11 de Mayo del 2020

**Aceptado:** 20 de Agosto del 2020

